A Survey on Self-Interference Cancellation in Mobile LTE-A/5G FDD Transceivers

Christian Motz, *Graduate Student Member, IEEE*, Thomas Paireder, *Graduate Student Member, IEEE*, Harald Pretl, *Senior Member, IEEE*, and Mario Huemer, *Senior Member, IEEE*

***Abstract*—This brief deals with self-interference (SI) effects in mobile communication radio frequency (RF) transceivers. The basics of current communication standards, namely Long-Term Evolution (LTE) and 5G, are outlined with a focus on carrier aggregation (CA). RF transceivers that support frequency-division duplex (FDD) and CA variants operate multiple receivers and transmitters simultaneously. We illustrate the resulting SI problems, present suitable models for different SI categories and discuss the associated interference estimation tasks. Moreover, we explain the basic architecture of two common countermeasures: digital and mixed-signal SI cancellation.**

***Index Terms*—Adaptive filters, interference cancellation, LTE, RF transceivers.**

I. Introduction

WIRELESS communication systems have gained increasing importance over the past decades. Advances in several areas including transmission and modulation schemes, coding, but also semiconductor manufacturing, enabled the remarkable development towards today's gigabit links [1]. Spectral efficiency is a key aspect for high data rates supported by current wireless communication standards such as Long-Term Evolution Advanced (LTE-A) or 5G [2], [3]. Highly integrated radio frequency (RF) transceivers [4], commonly based on the direct-conversion architecture [5], allow for cost-efficient mass production. Especially in mobile devices, they have to satisfy constraints in terms of form factor and power consumption. The integrated receive (Rx) and transmit (Tx) chains offer a high configuration flexibility to support a power efficient operation while simultaneously handling several communication standards. A general overview on transceiver implementations and their most important metrics is given in [6] and specific examples are presented in [7]–[16]. While current standards mainly build upon frequency-division duplex (FDD), in-band full-duplex (IBFD) transmission has become an active research area to push the limits further [17]–[22]. Obviously, the lack of separation in frequency leads to severe self-interference (SI) effects. The high interference power levels demand a combination of analog and digital countermeasures [23]–[26].

However, RF transceivers operating in FDD can also suffer from signal degradation due to SI effects – a less obvious fact. Basically, the Rx and Tx signals are separated by the duplex spacing defined by the band specifications. In addition, the analog front-end (AFE) contains band selection filters that achieve a limited isolation of typically 50 dB to 55 dB between Tx and Rx signals [27]–[29]. Filters with higher isolation are impractical due to several factors, such as insertion loss, cost and area. Considering the enormous Tx-Rx power difference of up to 120 dB, Tx leakage can still have a substantial power level in the Rx chains [30], [31]. Doubtlessly, an ideal Rx would not down-convert this leakage signal to the baseband (BB). Though, major building blocks of the Rx and Tx chains are based on analog circuitry showing unwanted nonlinear effects. This can generate new frequency components, potentially leading to a down-conversion of the leakage signal or a transformed version of it. In final consequence, the non-idealities result in a distortion of the wanted Rx signal. The negative impact can be limited but not avoided by design and, thus, is inherent to RF transceivers. Carrier aggregation (CA) complicates the situation even more since several Rx and Tx chains are operated simultaneously. This requires careful consideration of crosstalk effects [32]. Furthermore, CA results in even more stringent power and area constraints of the individual chains which affect the linearity negatively.

This brief aims to provide an introduction to SI in FDD transceivers. After recapitulating the basics of the LTE-A and 5G standards with a focus on CA in Section II, we explain the most important SI mechanisms in Section III. Moreover, in Section IV and Section V, respectively, suitable models and exemplary performance figures for digital and mixed-signal self-interference cancellation (SIC) architectures are discussed.

II. Fundamentals of Current Mobile Communication Standards

Current mobile communication standards build upon the orthogonal frequency-division multiplexing (OFDM) scheme. Long-Term Evolution (LTE) uses orthogonal

Manuscript received October 30, 2020; revised December 4, 2020; accepted December 30, 2020. Date of publication January 12, 2021; date of current version February 26, 2021. This work was support in part by the Austrian Federal Ministry for Digital and Economic Affairs; in part by the National Foundation for Research, Technology and Development; and in part by the Christian Doppler Research Association. This brief was recommended by Associate Editor J. M. de la Rosa. *(Corresponding author: Christian Motz.)*

Christian Motz, Thomas Paireder, and Mario Huemer are with the Christian Doppler Laboratory for Digitally Assisted RF Transceivers for Future Mobile Communications, Institute of Signal Processing, Johannes Kepler University Linz, 4040 Linz, Austria (e-mail: christian.motz@jku.at).

Harald Pretl is with the Institute for Integrated Circuits, Johannes Kepler University, 4040 Linz, Austria.

Color versions of one or more figures in this article are available at https://doi.org/10.1109/TCSII.2021.3051101.

Digital Object Identifier 10.1109/TCSII.2021.3051101

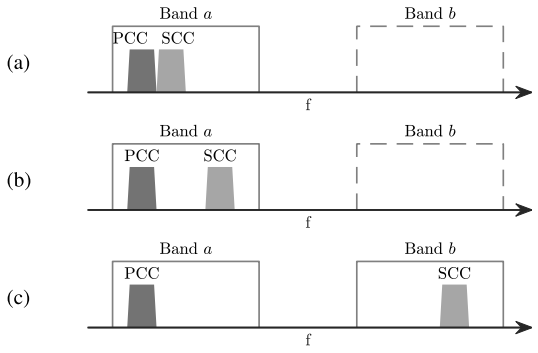

Fig. 1. Carrier aggregation variants defined by the LTE-A standard: intra-band contiguous (a), intra-band non-contiguous (b) and inter-band (c).

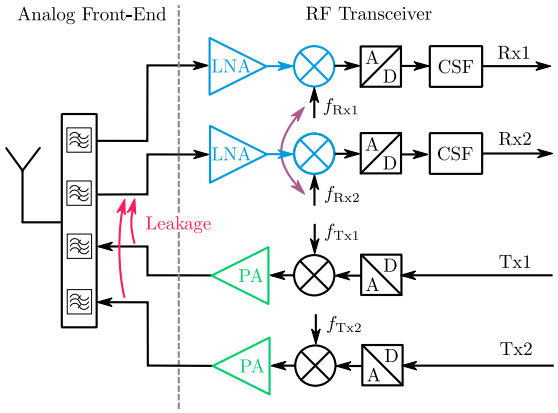

Fig. 2. Block diagram of FDD RF transceiver supporting CA.

frequency-division multiple access (OFDMA) for the downlink (DL) and single-carrier frequency-division multiple access (SC-FDMA)[1] for the uplink (UL). The second one is a variant of OFDMA with an additional data pre-coding to reduce the peak-to-average power ratio (PAPR). This is beneficial for battery-powered devices. The same holds for 5G, though here OFDMA is an alternative variant for the UL, too. Multi-carrier transmissions are advantageous because they allow for a dynamic resource sharing among multiple users. In case of LTE, frequency resources are managed in form of resource blocks (RBs), where one RB corresponds to 12 consecutive subcarriers. The overall number of RBs is determined by the channel bandwidth, which can be up to 20 MHz. In the time domain, LTE groups 7 OFDM symbols to form a slot. Many important parameters such as frequency resources, Tx power and data acknowledgment are managed on a slot basis. On a higher level, 20 slots form a radio frame. 5G keeps the basic topology but allows several parameters to be controlled on a symbol-by-symbol basis, which enables shorter latency and a more dynamic system. In addition, the subcarrier spacing is more flexible and not fixed to 15 kHz, like for LTE, and higher-order constellation mappings were added [3].

To achieve maximum data rates, several channels can be aggregated. This is termed CA and helps utilizing high bandwidths in the fragmented RF spectrum. Fig. 1 summarizes the three CA variants. First, intra-band contiguous CA adds secondary component carrier (SCC) in the same frequency band directly next to the primary component carrier (PCC). Second, intra-band non-contiguous CA allows to place the SCC anywhere in the same band as the PCC. Third, in inter-band CA, the PCC and the SCC can be placed flexibly in different bands [2]. Especially, the last two variants have influenced the implementation of RF transceivers by requiring the simultaneous operation of multiple Rx and Tx chains. This generated a new class of SI problems.

III. Self-Interference Effects in Detail

Fig. 2 shows the block diagram of a state-of-the-art FDD RF transceiver with two Rx and two Tx paths, supporting CA.

[1]Also known as DFT-precoded OFDMA (discrete Fourier transform pre-coded OFDMA) [3].

In addition to the shown band filters, the AFE contains RF switches to achieve the required flexibility. The basis for all SI effects is the frequency-selective Tx-Rx leakage path in the AFE highlighted in red. In the Tx chain, the power amplifier (PA), colored green, shows a relevant nonlinearity. In contrast, in the Rx chain, the nonlinearities typically result from a combination of the low-noise amplifier (LNA) and the mixer, highlighted in blue. Furthermore, the local oscillators (LOs) are usually fed by square waves, which together with crosstalk issues facilitate the occurrence of spur frequencies, indicated by the purple arrows. In the following, we will classify SI effects according to the underlying non-idealities and outline real-world cases. The focus is put on the resulting behavior and not on the exact source at circuit level, which heavily depends on the Rx and Tx topology. Reference [32] provides further details.

A. Receiver Nonlinearity

For modulated signals, a nonlinearity in the Rx inevitably generates intermodulation distortions (IMDs), such as IMD2 or IMD3. The nonlinearity is typically characterized by the second-order and third-order input intercept point (IIP2 and IIP3). Fig. 3(a) gives a schematic representation of this effect. The left side illustrates the involved RF signals in the frequency domain, whereas the right side shows the resulting impact on the BB spectra in the affected Rx chain. The IMD occurs regardless of a specific band or CA band combination, thus the figure shows a generic band a, where Rx and Tx operate on the carriers f_{Rx1} and f_{Tx1}, respectively. The rectangles indicate the restricted UL and DL frequency span of the band which typically is larger than the signal bandwidth. The BB contains the Rx1 signal and any down-converted IMD products that overlay the wanted signal. All RF signal components will produce this kind of distortion. Though, the overall IMD will be dominated by the strongest component, which is likely to be the Tx leakage.

B. Transmitter Nonlinearity

Besides other effects, a nonlinearity in the Tx creates signal components at harmonics of the Tx carrier frequency which might be a relevant problem in case of CA. Fig. 3(b) gives an

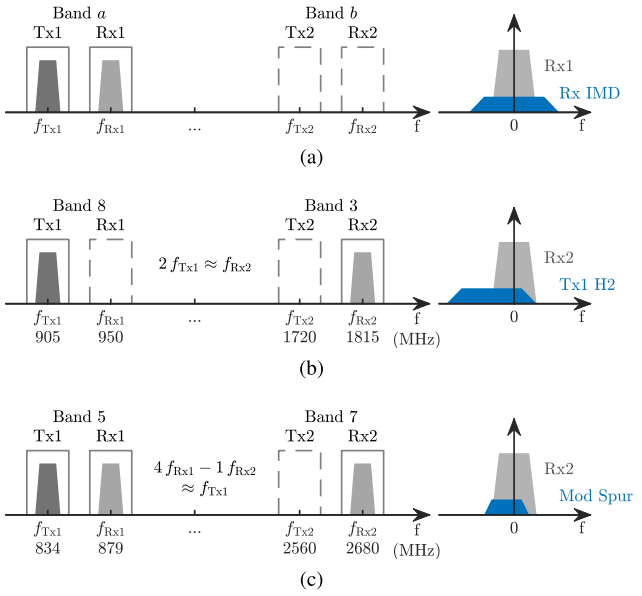

Fig. 3. Examples for different self-interference effects resulting from: receiver nonlinearity (a), transmitter nonlinearity (b) and spurious LOs (c).

example: Tx1 and Rx1 operate in band 8, whereas Rx2 operates in band 3. In fact, $2f_{\mathrm{Tx1}} = 1810\,\mathrm{MHz}$ almost coincides with $f_{\mathrm{Rx2}} = 1815\,\mathrm{MHz}$. As a result, the second harmonic of Tx1 overlays the wanted Rx2 in the BB. Moreover, the n-th harmonic has a bandwidth of $n \cdot B$, with B being the bandwidth of the undistorted signal. The problem even persists if only one of the active bands used for CA is FDD and the other are time-division duplex (TDD). Given the fact that LTE and 5G are commonly deployed within bands ranging from 410 MHz up to 7.1 GHz, the second and the third harmonic are most relevant. An example for a harmful distortion by the third harmonic would be CA operation in band 7 and 8.

C. Spurious LOs

Spurious LOs are a problem that specifically arises from the simultaneous operation of multiple Rx and Tx chains. The constraints on the RF transceiver in terms of power consumption and chip area make it hard to fully avoid crosstalk issues. In addition, frequency conversion is usually implemented using 50 % or 25 % duty-cycle passive mixers, where the LO signal is a square wave. This signal type exhibits a high number of harmonics with considerable power, which, in combination with a nonlinearity, can lead to the creation of continuous wave spurs. If such a spur in a down-conversion mixer LO signal is close to one of the Tx frequencies, the leakage signal will be down-converted unintentionally and distorts the wanted signal. This interference is known as modulated spur. Fig. 3(c) gives an example for a CA scenario with band 5 and 7. A spur frequency of $f_{\mathrm{sp}} = 4f_{\mathrm{Rx1}} - 1f_{\mathrm{Rx2}} = 836\,\mathrm{MHz}$ can arise, which almost coincides with $f_{\mathrm{Tx1}} = 834\,\mathrm{MHz}$. Consequently, the down-converted Tx1 leakage signal overlays the wanted Rx1 in BB. The same SI problem can result from a topology named split-LNA, which has a considerably low reverse isolation that facilitates problematic reflections and subsequent down-conversion [33].

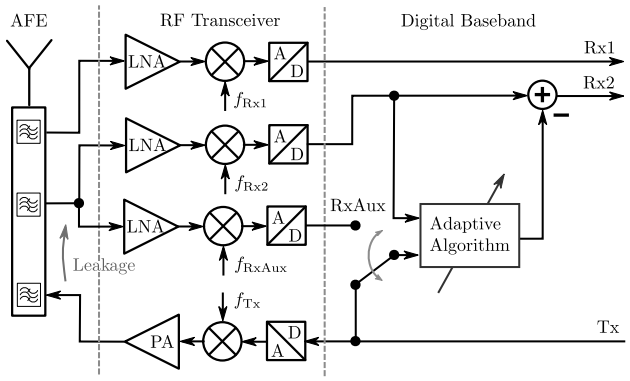

Fig. 4. Block diagram of FDD RF transceiver supporting CA. Additional blocks necessary for mixed-signal and digital SIC architectures are shown.

IV. Digital Self-Interference Cancellation

Despite the variety of effects, all SI signals are a function of a known Tx signal. The digital interference cancellation (DIC) architecture uses the Tx BB signal to replicate the interference. The basic principle is depicted in Fig. 4. The left part of the schematic shows the AFE and a typical RF transceiver supporting CA. The auxiliary (Aux) Rx path can be ignored for the moment and will be treated in Section V. The right part of the schematic contains the DIC scheme operating in the BB. All unknown parts of the interference mechanism, especially the time-varying and frequency-selective leakage path, have to be covered by an estimation process for a successful cancellation. This estimation is accomplished by an adaptive algorithm that uses the Tx BB and the Rx BB as input signals where the latter one does not only contain the wanted Rx signal but also the interference. Note that the adaptive algorithm has to operate on complex-valued data because the BB signals result from a double-sided spectrum in case of LTE or 5G.

A. Underlying Models and Estimation

Depending on the SI effect, an appropriate model has to be chosen for most DIC schemes. Doubtlessly, the model should fit the underlying interference effect by capturing all main aspects without being too generic. Consequently, this demands a precise understanding of the problem. Fig. 5 depicts three models for the SI effects explained in Section III. The model in Fig. 5a represents a linear finite impulse response (FIR) filter with an additional frequency shift. With appropriate filter weights, $w_1, \ldots, w_Q$, the relevant part of the frequency-selective leakage path can be replicated. This model is suitable for a modulated spur interference, which is created by spurious LOs as addressed above [34]. Tx nonlinearity requires a functional link model according to Fig. 5b. Here, a nonlinear function expansion $\mathbf{f}$: $\mathbb{C}^{\mathrm{P}} \rightarrow \mathbb{C}^{Q}$ is applied before the signals are combined linearly [35]. A precise modeling of the effect, e.g., spurious Tx emissions [36], [37] and Tx harmonics, yields an appropriate set of basis functions to construct this nonlinear mapping. Alternatively, a very generic set of basis functions could be chosen, which unfortunately, complicates the estimation process. The third variant is a Wiener model according to Fig. 5c, where the signal passes a linear

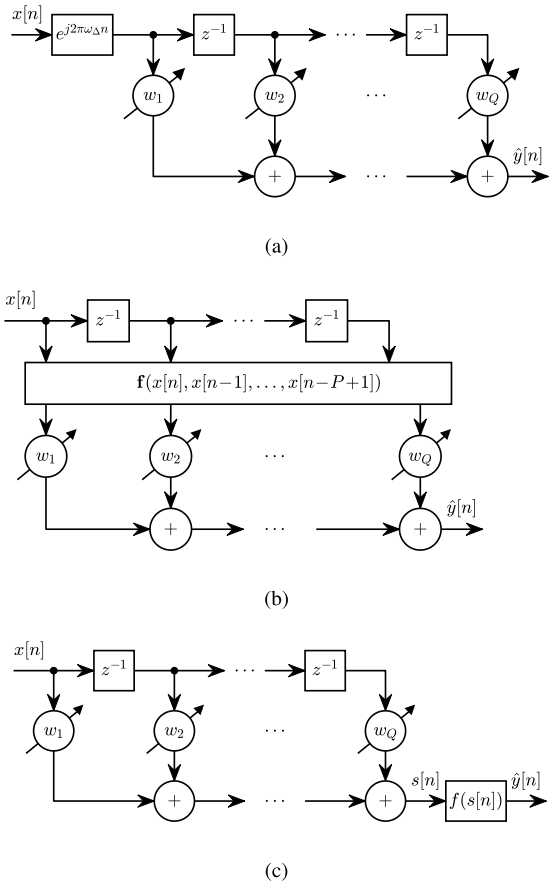

Fig. 5. Linear (a), functional link (b) and Wiener (c) models appropriate for different SI effects.

FIR filter and is then transformed by a nonlinear mapping $f\colon \mathbb{C} \to \mathbb{C}$ [38]. This model satisfies the requirements of Rx nonlinearity interference effects, where the frequency-shaped leakage signal undergoes a nonlinearity. The filter weights, and possibly the parameters of the nonlinearity, have to be estimated.

The parameter estimation is performed on a sample- or block-adaptive basis. The linear model in Fig. 5a can be estimated by sample-adaptive standard methods, such as the least-mean squares (LMS) algorithm based on the stochastic gradient descent (SGD) concept, or the recursive least squares (RLS) algorithm [39], [40]. Block based solutions usually build upon the standard least squares (LS) algorithm. Besides SIC based on the normalized LMS (N-LMS) and RLS, modified variants of the LMS have been used successfully [34], [41]–[44]. The model shown in Fig. 5b, even though being a nonlinear structure, represents a linear estimation problem, too. Reference [36], [45] build upon this kind of model and solve the estimation problem with the standard LS algorithm, whereas [46] employs a sample-adaptive method. The Wiener model according to Fig. 5c is more difficult to handle. In [47], [48], nonlinear LMS and RLS like adaptive algorithms are derived for IMD2 resulting from Rx nonlinearity.

In contrast to model-based solutions, these problems can also be solved by neural networks [49]–[52], kernel methods [53], spline-interpolation based methods [54] or support vector machines [55]. For general information on methods for nonlinear system identification we refer the reader to [56].

The performance of the estimation algorithm is only one aspect; doubtlessly, a real-time capable implementation is of equal importance. Consequently, low-cost algorithms like the LMS are preferred because their low computational complexity matches best with constraints in terms of chip area and power consumption. However, LTE signals have challenging statistics for SGD-based algorithms [44]. RLS-based algorithms are more robust in this respect, but require careful consideration of numeric stability. Nonetheless, low-cost implementations that fulfill this property are possible [57]. Another aspect is the feedback-based nature of the adaptive filters, which complicates a pipelined hardware design. The resulting delayed update has to be considered and imposes certain constraints on the parameters to guarantee stability [58].

B. Performance

The performance of SIC algorithms depends on many system parameters, rendering it difficult to compare the performance numbers found in literature (see Section IV-A). In order to enable a fair comparison of SIC architectures, we established a unified simulation setup for the modulated spur problem [44], which is used as an example throughout this brief. For comparisons of further SIC algorithms, we refer to [59]–[61]. We start with the DIC scheme, whereas mixed-signal interference cancellation (MSIC) follows in Section V-B. The adaptive filter order Q is set to 16, which proved to be a suitable compromise in our simulations. The leakage path models are based on measurements from real-world duplexers. The SIC architecture is the same as in Fig. 4, and four different adaptive filters are applied for comparison. Tx1 is chosen to be an LTE-20 signal with 10 RBs allocated. The signal-to-interference-plus-noise ratio (SINR) according to

$$\mathrm{SINR} = \frac{\mathrm{E}\left[|y_{\mathrm{Rx}}[n]|^2\right]}{\mathrm{E}\left[\left|y_{\mathrm{Int}}[n] - \hat{y}_{\mathrm{Int}}[n] + \eta[n]\right|^2\right]}, \tag{1}$$

is used as the performance metric. $y_{\mathrm{Rx}}[n]$ represents the wanted Rx signal (in this example LTE-20, fully allocated). $y_{\mathrm{Int}}[n]$, $\hat{y}_{\mathrm{Int}}[n]$ and $\eta[n]$ are the interference, the estimated interference and the noise, respectively. In the ideal case, the interference is either not present or is perfectly compensated by the estimated interference and the SINR reduces to the signal-to-noise ratio (SNR). In any other case, the SINR represents the SNR degradation resulting from the remaining interference after cancellation.

Fig. 6 shows the ensemble-averaged results in the steady-state for varying interference-to-carrier-plus-noise (ICN) ratios

$$\mathrm{ICN} = \frac{\mathrm{E}\left[|y_{\mathrm{Int}}[n]|^2\right]}{\mathrm{E}\left[|y_{\mathrm{Rx}}[n] + \eta[n]|^2\right]}. \tag{2}$$

This metric relates the power of the interference to the combined power of the wanted Rx and the noise. In addition to the

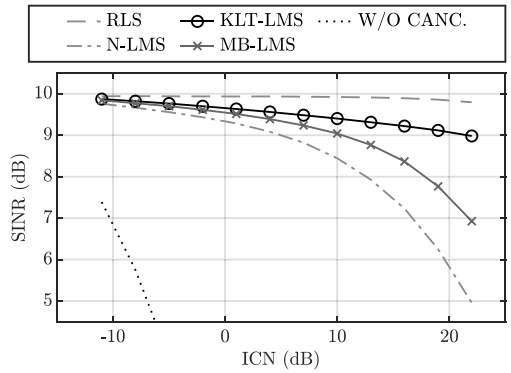

Fig. 6. SINR improvement of different digital modulated spur SIC schemes in the steady-state [44].

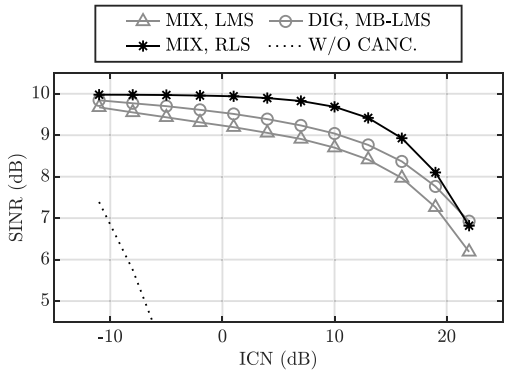

Fig. 7. SINR improvement of different modulated spur SIC architectures in the steady-state [70].

N-LMS and the RLS, Fig. 6 includes the model-based (MB)-LMS and the Karhunen-Loève transform (KLT)-LMS, which have specifically been designed for this application and incorporate LTE signal statistics [44]. Doubtlessly, a higher ICN requires a better cancellation, which is challenging for SGD-based algorithms. While the RLS gives the best performance, it is not feasible for real-time implementation in this application due to its computational complexity. It is only included as a reference. The N-LMS shows the weakest cancellation, especially for higher ICN values, but has the lowest computational complexity. The MB-LMS features considerably better results for some increase in computational costs. Finally, the KLT-LMS comes relatively close to the RLS at moderate complexity. Consequently, these two specific LMS variants are the best options in this comparison. On the contrary, the two standard adaptive filters (N-LMS, RLS) are suboptimal in this scenario.

V. Mixed-Signal Interference Cancellation

The basic principle of MSIC is depicted in Fig. 4. In contrast to DIC, an Aux Rx path is employed that feeds the adaptive algorithm. The idea is to capture the leakage signal including the frequency shaping of the Tx-Rx leakage path. Consequently, the Aux Rx is typically tuned to the appropriate frequency for the leakage effect. The Aux Rx also captures phase noise resulting from the frequency conversion in the Tx path, which cannot be achieved by DIC [33]. Several MSIC approaches are not limited to SI but additionally target external interferers.

A crucial factor for MSIC is designing the Aux Rx. Of course, the circuit design of a main Rx chain could be reused. However, the requirements can be relaxed to optimize area and power consumption. A suitable Aux Rx design including an experimental verification is provided in [62]. However, the I/Q imbalance of this simplified Rx can limit the feasible cancellation performance. This problem can be alleviated by appropriate processing of the Aux Rx BB data [63].

Especially for the modulated spur problem, more specific Aux Rx designs have been proposed that mimic the building law for spurious LOs. The serial mixing concept down-converts the RF signal by a series of mixers which are fed by the involved LO signals [33], [64], [65].

Another variant of MSIC is employing an Aux Tx. This enables direct RF level cancellation and prevents the analog-to-digital converter (ADC) in the Rx chain from saturation even at high interference levels [66]. This concept is especially vital for IBFD.

A. Underlying Models and Estimation

Employing an Aux Rx typically simplifies the estimation problem compared to DIC architectures. The model in Fig. 5a satisfies the requirements for the modulated spur problem. In contrast to DIC, the filter order Q can be much lower because the filter does not have to capture the frequency shaping of the Tx-Rx leakage path. Instead, only minor amplitude and phase mismatches between the main and the Aux Rx paths have to be compensated. Standard LMS and RLS-based estimation methods have been applied successfully [33], [62], [64]. The multi-phase mixing concept builds upon the same principle but chains multiple of these models and cancels the individual interferers step by step [67].

MSIC has also been successfully used to cancel IMD resulting from Rx nonlinearities by employing a model according to Fig. 5b. In [65], a modulated spur and resulting IMD2 components are canceled simultaneously. In [68], [69], multiple even-order IMD components in the Rx are canceled. The proposed scheme can be applied to external interferers, too.

B. Performance

Again, we focus on the modulated spur problem to assess the performance of MSIC schemes according to [70]. The simulation setup is identical to the one used in Section IV. MSIC employs the LMS and the RLS for comparison. Note that, here, the RLS is a realistic option for implementation due to the low adaptive filter order $Q = 3$. The MB-LMS variant of the DIC architecture serves as the reference. Fig. 7 depicts the results. In addition, the dashed line shows the SINR degradation without cancellation. Doubtlessly, even low ICN values require countermeasures, otherwise throughput suffers severely or decoding becomes challenging for negative SINR values. The MSIC approach combined with an RLS gives best performance, though the LMS gives reasonable performance, too. For high ICN values both MSIC variants suffer from some

performance degradation. In this region, the performance of the Aux Rx, which was assumed to have an SNR of 30 dB, is the limiting factor. In summary, both the DIC and the MSIC architecture can provide a sufficient level of cancellation for the modulated spur problem provided that an appropriate adaptive filter is chosen. The analysis highlights that, in general, there is no single optimal solution to a given SI problem.

VI. Conclusion

In this brief, we explained the most important SI effects, such as modulated spurs (caused by LO harmonics and crosstalk), Rx IMD and Tx harmonics. In addition, we gave a concise overview of suitable models and the underlying estimation problems for SIC. Finally, we presented the basics of digital as well as mixed-signal cancellation architectures including performance and aspects of implementation.

References

[1] S. Kanchi, S. Sandilya, D. Bhosale, A. Pitkar, and M. Gondhalekar, "Overview of LTE-A technology," in *Proc. IEEE Global High Tech Congr. Electron.*, 2013, pp. 195–200.

[2] E. Dahlman, S. Parkvall, and J. Skold, *4G: LTE/LTE-Advanced for Mobile Broadband*. Amsterdam, The Netherlands: Elsevier Sci., 2013.

[3] E. Dahlman, S. Parkvall, and J. Skold, *5G NR: The Next Generation Wireless Access Technology*. Amsterdam, The Netherlands: Elsevier Sci., 2018.

[4] S. Bronckers, A. Roc'h, and B. Smolders, "Wireless receiver architectures towards 5G: Where are we?" *IEEE Circuits Syst. Mag.*, vol. 17, no. 3, pp. 6–16, 2017.

[5] B. Razavi, "Design considerations for direct-conversion receivers," *IEEE Trans. Circuits Syst. II, Analog Digit. Signal Process.*, vol. 44, no. 6, pp. 428–435, Jun. 1997.

[6] P. Baudin, *Wireless Transceiver Architecture: Bridging RF and Digital Communications*. Chichester, U.K.: Wiley, 2014.

[7] H. Xie *et al.*, "Single-chip multiband EGPRS and SAW-less LTE WCDMA CMOS receiver with diversity," *IEEE Trans. Microw. Theory Techn.*, vol. 60, no. 5, pp. 1390–1396, May 2012.

[8] N. Klemmer *et al.*, "A 45nm CMOS RF-to-bits LTE/WCDMA FDD/TDD 2A—2 MIMO base-station transceiver SoC with 200MHz RF bandwidth," in *Proc. IEEE Int. Solid-State Circuits Conf. (ISSCC)*, 2016, pp. 164–165.

[9] M. Mikhemar *et al.*, "A rel-12 2G/3G/LTE-advanced 3CC cellular receiver," *IEEE J. Solid-State Circuits*, vol. 51, no. 5, pp. 1066–1079, May 2016.

[10] S. Singh, M. Valkama, M. Epp, and W. Schlecker, "Digitally enhanced wideband I/Q downconversion receiver with 2-channel time-interleaved ADCs," *IEEE Trans. Circuits Syst. II, Exp. Briefs*, vol. 63, no. 1, pp. 29–33, Jan. 2016.

[11] B. Mohammadi *et al.*, "A rel-12 2G/3G/LTE-advanced 2CC transmitter," *IEEE J. Solid-State Circuits*, vol. 51, no. 5, pp. 1080–1095, May 2016.

[12] C. Chiu *et al.*, "A 40nm low-power transceiver for LTE-A carrier aggregation," in *Proc. IEEE Int. Solid-State Circuits Conf. (ISSCC)*, 2017, pp. 130–131.

[13] T. Wu *et al.*, "A 40nm 4-downlink and 2-uplink RF transceiver supporting LTE-Advanced carrier aggregation," in *Proc. IEEE Radio Freq. Integr. Circuits Symp. (RFIC)*, 2018, pp. 316–319.

[14] B. Jann *et al.*, "A 5G sub-6GHz zero-IF and mm-Wave IF transceiver with MIMO and carrier aggregation," in *Proc. IEEE Int. Solid-State Circuits Conf. (ISSCC)*, 2019, pp. 352–354.

[15] C. Tang *et al.*, "An LTE-A multimode multiband RF transceiver with 4RX/2TX inter-band carrier aggregation, 2-carrier 4A—4 MIMO with 256QAM and HPUE capability in 28nm CMOS," in *Proc. IEEE Int. Solid-State Circuits Conf. (ISSCC)*, 2019, pp. 350–352.

[16] J. Lee *et al.*, "A sub-6-GHz 5G new radio RF transceiver supporting EN-DC with 3.15-Gb/s DL and 1.27-Gb/s UL in 14-nm FinFET CMOS," *IEEE J. Solid-State Circuits*, vol. 54, no. 12, pp. 3541–3552, Dec. 2019.

[17] D. Korpi, L. Anttila, and M. Valkama, "Feasibility of in-band full-duplex radio transceivers with imperfect RF components: Analysis and enhanced cancellation algorithms," in *Proc. 9th Int. Conf. Cogn. Radio Orient. Wireless Netw. Commun. (CROWNCOM)*, 2014, pp. 532–538.

[18] A. Sabharwal, P. Schniter, D. Guo, D. W. Bliss, S. Rangarajan, and R. Wichman, "In-band full-duplex wireless: Challenges and opportunities," *IEEE J. Sel. Areas Commun.*, vol. 32, no. 9, pp. 1637–1652, Sep. 2014.

[19] D. Kim, H. Lee, and D. Hong, "A survey of in-band full-duplex transmission: From the perspective of PHY and MAC layers," *IEEE Commun. Surveys Tuts.*, vol. 17, no. 4, pp. 2017–2046, 4th Quart., 2015.

[20] Z. Zhang, K. Long, A. V. Vasilakos, and L. Hanzo, "Full-duplex wireless communications: Challenges, solutions, and future research directions," *Proc. IEEE*, vol. 104, no. 7, pp. 1369–1409, Jul. 2016.

[21] T. Riihonen, D. Korpi, O. Rantula, H. Rantanen, T. Saarelainen, and M. Valkama, "Inband full-duplex radio transceivers: A paradigm shift in tactical communications and electronic warfare?" *IEEE Commun. Mag.*, vol. 55, no. 10, pp. 30–36, Oct. 2017.

[22] K. E. Kolodziej, B. T. Perry, and J. S. Herd, "In-band full-duplex technology: Techniques and systems survey," *IEEE Trans. Microw. Theory Techn.*, vol. 67, no. 7, pp. 3025–3041, Jul. 2019.

[23] D. Korpi, L. Anttila, and M. Valkama, "Nonlinear self-interference cancellation in MIMO full-duplex transceivers under crosstalk," *EURASIP J. Wireless Commun. Netw.*, Feb. 2017, Art. no. 24.

[24] D. Korpi, T. Riihonen, L. Anttila, and M. Valkama, "Self-interference modeling and digital cancellation along with full-duplex wireless system analysis," in *Proc. Int. Conf. Signal Process. Commun. (SPCOM)*, 2018, pp. 432–436.

[25] M. Bernhardt, F. Gregorio, J. Cousseau, and T. Riihonen, "Self-interference cancelation through advanced sampling," *IEEE Trans. Signal Process.*, vol. 66, no. 7, pp. 1721–1733, Apr. 2018.

[26] M. Aghababaeetafreshi, D. Korpi, M. Koskela, P. Jääskeläinen, M. Valkama, and J. Takala, "Software defined radio implementation of a digital self-interference cancellation method for inband full-duplex radio using mobile processors," *J. Signal Process. Syst.*, vol. 90, no. 10, pp. 1297–1309, 2018.

[27] M. Mikhemar, H. Darabi, and A. Abidi, "A tunable integrated duplexer with 50dB isolation in 40nm CMOS," in *Proc. IEEE Int. Solid-State Circuits Conf. Dig. Tech. Papers*, 2009, pp. 386–387.

[28] M. Mikhemar, H. Darabi, and A. A. Abidi, "A multiband RF antenna duplexer on CMOS: Design and performance," *IEEE J. Solid-State Circuits*, vol. 48, no. 9, pp. 2067–2077, Sep. 2013.

[29] "Saw duplexer, LTE/WCDMA band 3, series: B8625," TDK, Tokyo, Japan, Data Sheet, 2014. [Online]. Available: http://static6.arrow.com/aropdfconversion/d02a7e8b179789d6426087c1ffa6fa33cd180f0f/b8625.pdf

[30] *Evolved Universal Terrestrial Radio Access (E-UTRA); User Equipment (UE) Radio Transmission and Reception, Version 14.5.0*, 3GPP Standard TS 36.101, Nov. 2017.

[31] *5G; NR; User Equipment (UE) Radio Transmission and Reception; Part 1: Range 1 Standalone, Version 15.3.0*, 3GPP Standard TS 36.101, Oct. 2018.

[32] S. Sadjina, C. Motz, T. Paireder, M. Huemer, and H. Pretl, "A survey of self-interference in LTE-Advanced and 5G new radio wireless transceivers," *IEEE Trans. Microw. Theory Techn.*, vol. 68, no. 3, pp. 1118–1131, Mar. 2020.

[33] S. Sadjina, R. S. Kanumalli, A. Gebhard, K. Dufréne, M. Huemer, and H. Pretl, "A mixed-signal circuit technique for cancellation of interferers modulated by LO phase-noise in 4G/5G CA transceivers," *IEEE Trans. Circuits Syst. I, Reg. Papers*, vol. 65, no. 11, pp. 3745–3755, Nov. 2018.

[34] A. Gebhard, R. S. Kanumalli, B. Neurauter, and M. Huemer, "Adaptive self-interference cancelation in LTE-A carrier aggregation FDD direct-conversion transceivers," in *Proc. IEEE Sensor Array Multichannel Signal Process. Workshop (SAM)*, Jul. 2016, pp. 1–5.

[35] D. Comminiello, M. Scarpiniti, L. A. Azpicueta-Ruiz, J. Arenas-Garcia, and A. Uncini, "Functional link adaptive filters for nonlinear acoustic echo cancellation," *IEEE Trans. Audio, Speech, Language Process.*, vol. 21, no. 7, pp. 1502–1512, Jul. 2013.

[36] A. Kiayani, L. Anttila, and M. Valkama, "Modeling and dynamic cancellation of TX-RX leakage in FDD transceivers," in *Proc. IEEE 56th Int. Midwest Symp. Circuits Syst. (MWSCAS)*, Aug. 2013, pp. 1089–1094.

[37] A. Kiayani, V. Lehtinen, L. Anttila, T. Lahteensuo, and M. Valkama, "Linearity challenges of LTE-advanced mobile transmitters: Requirements and potential solutions," *IEEE Commun. Mag.*, vol. 55, no. 6, pp. 170–179, 2017.

[38] T. Ogunfunmi, *Adaptive Nonlinear System Identification: The Volterra and Wiener Model Approaches* (Signals and Communication Technology). New York, NY, USA: Springer, 2007.

[39] A. H. Sayed, *Fundamentals of Adaptive Filtering*. New York, NY, USA: Wiley, 2003.

[40] P. S. Diniz, *Adaptive Filtering: Algorithms and Practical Implementation*, 2nd ed. Boston, MA, USA: Kluwer, 2002.

[41] R. S. Kanumalli, A. Gebhard, A. Elmaghraby, A. Mayer, D. Schwartz, and M. Huemer, "Active digital cancellation of transmitter induced modulated spur interference in 4G LTE carrier aggregation transceivers," in *Proc. IEEE 83rd Veh. Technol. Conf. (VTC Spring)*, May 2016, pp. 1–5.

[42] R. S. Kanumalli *et al.*, "Digitally-intensive transceivers for future mobile communications - emerging trends and challenges," *E & I Elektrotechnik und Informationstechnik*, vol. 135, no. 1, pp. 30–39, Feb. 2018.

[43] C. Motz, O. Ploder, T. Paireder, and M. Huemer, "Enhanced transform-domain LMS based self-interference cancellation in LTE carrier aggregation transceivers," in *Computer-Aided Systems Theory—EUROCAST 2019* (Lecture Notes in Computer Science). Cham, Switzerland: Springer, 2020.

[44] C. Motz, T. Paireder, and M. Huemer, "Improving digital interference cancellation in LTE-A/5G-transceivers by statistical modeling," in *Proc. 54th Asilomar Conf. Signals Syst. Comput.*, to be published.

[45] A. Kiayani, L. Anttila, M. Kosunen, K. Stadius, J. Ryynänen, and M. Valkama, "Modeling and joint mitigation of TX and RX nonlinearity-induced receiver desensitization," *IEEE Trans. Microw. Theory Techn.*, vol. 65, no. 7, pp. 2427–2442, Jul. 2017.

[46] S. Lahti, P. P. Campo, V. Lampu, L. Anttila, M. Valkama, and T. D. Hämäläinen, "Implementation of a nonlinear self-interference canceller using high-level synthesis," in *Proc. IEEE Int. Symp. Circuits Syst. (ISCAS)*, 2020, pp. 1–5.

[47] A. Gebhard, C. Motz, R. S. Kanumalli, H. Pretl, and M. Huemer, "Nonlinear least-mean-squares type algorithm for second-order interference cancellation in LTE-A RF transceivers," in *Proc. IEEE 51st Asilomar Conf. Signals Syst. Comput.*, Oct. 2017, pp. 802–807.

[48] A. Gebhard *et al.*, "A robust nonlinear RLS type adaptive filter for second-order-intermodulation distortion cancellation in FDD LTE and 5G direct conversion transceivers," *IEEE Trans. Microw. Theory Techn.*, vol. 67, no. 5, pp. 1946–1961, May 2019.

[49] O. Ploder, O. Lang, T. Paireder, and M. Huemer, "An adaptive machine learning based approach for the cancellation of second-order-intermodulation distortions in 4G/5G transceivers," in *Proc. IEEE 90th Veh. Technol. Conf. (VTC-Fall)*, 2019, pp. 1–7.

[50] O. Ploder, C. Motz, T. Paireder, and M. Huemer, "A neural network approach for the cancellation of the second-order-intermodulation distortion in future cellular RF transceivers," in *Proc. 53rd Asilomar Conf. Signals Syst. Comput.*, 2019, pp. 1144–1148.

[51] A. T. Kristensen, A. Burg, and A. Balatsoukas-Stimming, "Advanced machine learning techniques for self-interference cancellation in full-duplex radios," in *Proc. 53rd Asilomar Conf. Signals Syst. Comput.*, 2019, pp. 1149–1153.

[52] Y. Kurzo, A. T. Kristensen, A. Burg, and A. Balatsoukas-Stimming, "Hardware implementation of neural self-interference cancellation," *IEEE J. Emerg. Sel. Topics Circuits Syst.*, vol. 10, no. 2, pp. 204–216, Jun. 2020.

[53] C. Auer, T. Paireder, O. Lang, and M. Huemer, "Kernel recursive least squares based cancellation for receiver-induced self-interference," in *Proc. 54th Asilomar Conf. Signals Syst. Comput.*, to be published.

[54] P. P. Campo, L. Anttila, D. Korpi, and M. Valkama, "Adaptive cancellation of nonlinear self-interference in wireless full-duplex: Cascaded spline-interpolated methods," in *Proc. 54th Asilomar Conf. Signals Syst. Comput.*, to be published.

[55] C. Auer, K. Kostoglou, T. Paireder, O. Ploder, and M. Huemer, "Support vector machines for self-interference cancellation in mobile communication transceivers," in *Proc. IEEE 91st Veh. Technol. Conf. (VTC-Spring)*, 2020, pp. 1–6.

[56] D. Comminiello and J. Principe, Eds., *Adaptive Learning Methods for Nonlinear System Modeling*. Amsterdam, The Netherlands: Elsevier Sci., 2018.

[57] P. Monsurró and A. Trifiletti, "Faster, stabler, and simpler—A recursive-least-squares algorithm exploiting the Frisch–Waugh–Lovell theorem," *IEEE Trans. Circuits Syst. II, Exp. Briefs*, vol. 64, no. 3, pp. 344–348, Mar. 2017.

[58] M. Rupp and R. Frenzel, "Analysis of LMS and NLMS algorithms with delayed coefficient update under the presence of spherically invariant processes," *IEEE Trans. Signal Process.*, vol. 42, no. 3, pp. 668–672, Mar. 1994.

[59] A. Gebhard, "Self-interference cancellation and rejection in FDD RF-transceivers," Ph.D. dissertation, Doktor der technischen Wissenschaften, Johannes Kepler Univ. Linz, Linz, Austria, 2019. [Online]. Available: https://resolver.obvsg.at/urn:nbn:at:at-ubl:1-28339

[60] S. A. Sadjina, "Mixed-signal interference mitigation in cellular receivers," Ph.D. dissertation, Doktor der technischen Wissenschaften, Johannes Kepler Univ. Linz, Linz, Austria, 2019. [Online]. Available: https://resolver.obvsg.at/urn:nbn:at:at-ubl:1-32822

[61] R. S. Kanumalli, "Interference cancellation in 4G/5G cellular modems," Ph.D. dissertation, Johannes Kepler Univ. Linz, Johannes Kepler Univ. Linz, Linz, Austria, 2020.

[62] A. Elmaghraby *et al.*, "A mixed-signal technique for TX-induced modulated spur cancellation in LTE-CA receivers," *IEEE Trans. Circuits Syst. I, Reg. Papers*, vol. 65, no. 9, pp. 3060–3073, Sep. 2018.

[63] R. S. Kanumalli *et al.*, "Mixed-signal based enhanced widely linear cancellation of modulated spur interference in LTE-CA transceivers," in *Proc. 52nd Asilomar Conf. Signals Syst. Comput.*, 2018, pp. 1382–1388.

[64] S. Sadjina, D. Krzysztof, R. S. Kanumalli, M. Huemer, and H. Pretl, "A circuit technique for blocker-induced modulated spur cancellation in 4G LTE carrier aggregation transceivers," in *Proc. Austrochip Workshop Microelectron.*, Oct. 2017, pp. 23–28.

[65] S. Sadjina, D. Krzysztof, R. S. Kanumalli, M. Huemer, and H. Pretl, "Interference mitigation in LTE-CA FDD based on mixed-signal widely linear cancellation," in *Proc. 22nd Int. Microwave Radar Conf. (MIKON)*, May 2018, pp. 558–561.

[66] A. Kiayani *et al.*, "Adaptive nonlinear RF cancellation for improved isolation in simultaneous transmit–receive systems," *IEEE Trans. Microw. Theory Techn.*, vol. 66, no. 5, pp. 2299–2312, May 2018.

[67] S. Sadjina, K. Dufrêne, R. S. Kanumalli, M. Huemer, and H. Pretl, "21.7 A mixed-signal circuit technique for cancellation of multiple modulated spurs in 4G/5G carrier-aggregation transceivers," in *Proc. IEEE Int. Solid-State Circuits Conf. (ISSCC)*, 2019, pp. 356–358.

[68] E. A. Keehr and A. Hajimiri, "Successive regeneration and adaptive cancellation of higher order intermodulation products in RF receivers," *IEEE Trans. Microw. Theory Techn.*, vol. 59, no. 5, pp. 1379–1396, May 2011.

[69] T. Paireder, C. Motz, S. Sadjina, and M. Huemer, "A robust mixed-signal cancellation approach for even-order intermodulation distortions in LTE-A/5G-transceivers," *IEEE Trans. Circuits Syst. II, Exp. Briefs*, early access, Sep. 8, 2020, doi: 10.1109/TCSII.2020.3022918.

[70] C. Motz, T. Paireder, and M. Huemer, "Modulated spur interference cancellation for LTE-A/5G transceivers: A system level analysis," in *Proc. IEEE 91st Veh. Technol. Conf. (VTC Spring)*, May 2020, pp. 1–6.